The Ablation and Oxidation Behaviors of SiC Coatings on Graphite Prepared by Slurry Sintering and Pack Cementation

Reza Aliasgarian, Malek Naderi, Seyyed Ehsan Mirsalehi, and Saeed Safi

SiC coatings were generated on graphite using slurry sintering (SS) and pack cementation (PC). The samples' ablation features were assessed by an oxyacetylene torch. The rates of mass ablation of the PC–SiC and SS–SiC coatings were approximated 2.17×10^{-3} and 9.52×10^{-3} g s^{-1}, respectively, decreased by 84.1 and 29.6% compared to the uncoated samples. It was mainly attributed to the formation of a SiO_2 layer on the surface. The continuous SiO_2 molten film formed via the PC–SiC oxidation generates a sealing mechanism which can be an obstacle against the oxygen diffusion and hinder more ablation. This is while discontinuous SiO_2 film formed from the thin SS–SiC cannot protect the graphite effectively. The non-isothermal oxidation test shows that without the SiC coating, the sample weight is lost largely from 25 to 1500 °C, and its weight loss was 2.2% after the TGA. However, after coating, the samples possessed excellent oxidation protection and weight losses of SS–SiC and PC–SiC coatings are down to 1.3 and 0.6%, respectively. The more oxidation of the graphite substrate occurred due to the formation of macrocracks in the coating during the TGA and also the formation of holes on SiO_2 glass layer owing to release of CO or CO_2.

1. Introduction

Graphite is one of the attractive materials in high-temperature applications because of its high strength, high modulus, low density and excellent thermal shock resistance (Ref 1-4). However, these materials oxidize at temperatures above 500 °C, which restricts their applications (Ref 5-7). Therefore, oxidation protection is essential in an oxygen environment at high temperature. To prevent carbon materials from ablation and oxidation at high temperature, various kinds of ceramic coatings have been explored (Ref 8-12). Among these coatings, SiC is one of the best coatings due to its good anti-oxidation property, high mechanical properties and low density (Ref 13-16). Various techniques have been employed to prepare SiC coating on carbon materials, such as slurry sintering (SS) (Ref 17), pack cementation (PC) (Ref 18), and chemical vapor deposition (CVD) (Ref 19, 20). So far, several studies have been conducted to investigate the oxidation resistance of SiC coating prepared by PC (Ref 7, 15, 19, 21-24). The PC–SiC coating provided excellent oxidation resistance, proving able to protect C/C composites from oxidation for more than 310 h at 1773 K in the air (Ref 14). Compared oxidation resistance of SiC coatings prepared by CVD and PC, the oxidation resistance of the PC–SiC coating was better than that of the CVD–SiC

coating at elevated temperatures (Ref 19). A few studies have investigated the oxidation resistance of coatings produced by SS (Ref 4, 17, 25-27). It was found by Zhao et al. that the pore radius of graphite has marked effect on the oxidation resistance of SiC coating prepared by SS (Ref 17). In another study, results show that the sintering temperature has an important effect on the thickness and resistance against irradiation of the SiC coatings (Ref 25). In spite of numerous studies on the oxidation behavior of SiC coating by isothermal and thermal shock tests, a few studies have been conducted under non-isothermal oxidation. Also, there are a few papers about ablation behavior of SiC coatings (Ref 12, 28, 29). Ni et al. identified ablation mechanism of SiC-coated C/C composites at 0° angle in two flame conditions under an oxyacetylene flame (Ref 29). Yang et al. concluded that the SiC coating has a good ablation resistance for short time (Ref 12). Considering the above, further research is needed to determine the ablation property and ablation mechanism of SiC coatings.

In this research, two types of SiC coatings were produced on the graphite by slurry-sintering and pack cementation methods. The coating's ablation resistance was examined using an oxyacetylene torch. The ablation mechanism and properties were assessed. The coating's non-isothermal oxidation performances from the room temperature to 1500 °C were studied.

2. Experimental

The specimens, with a dimension of Φ 30 mm × 10 mm and 10 × 10 × 10 mm³, were separated from graphite bulk with 1.8 g/cm³ density. The samples were hand-abraded by grit SiC paper 320, 800 and 2400. Afterward, they were dried for 2 h at 100 °C and cleaned with distilled water. The SiC coating was produced by slurry-sintering and pack cementation meth-

Reza Aliasgarian, Malek Naderi, and Seyyed Ehsan Mirsalehi, Department of Mining and Metallurgical Eng, Amirkabir University of Technology, Tehran, Iran; and Saeed Safi, Ceramic Department, Materials and Energy Research Center, Karaj, Iran. Contact e-mail: mnaderi@aut.ac.ir.

ods. A powder mixture consisted of 30 wt.% Si, 60 wt.% SiC, and 10 wt.% Al_2O_3 in the pack cementation approach. In a crucible, the graphite samples were immersed in the powder mixture; afterward, they were heat-treated in the vacuum atmosphere for 3 h at 1700 °C.

In preparing SiC coating by slurry sintering, Si powder with average sizes of 10 μm was blended with alcohol and phenolic resin in a ball mill for 2 h. The slurry was painted on the specimen and then was allowed to dry for 1 h at 100 °C. After drying, coated specimens were sintered at 1700 °C for 3 h in a vacuum furnace.

The ablation features of specimens were assessed with the system of an oxyacetylene torch. The pressure and flux of C_2H_2 were 0.095 MPa and 0.31 L/s, and for O_2 were 0.4 MPa and 0.42 L/s, respectively. For 60 s, the specimens were put on to the flame. The internal diameter of the tip of the nozzle was 2.0 mm, and the distance between the samples and the nozzle tip was 10 mm. The central surface's temperature was obtained using an optical pyrometer during the ablation. The mass and linear ablation rates of the specimens were achieved based on the following equations:

$$R_m = (\Delta m)/t \qquad (Eq\ 1)$$

$$R_1 = (\Delta d)/t \qquad (Eq\ 2)$$

where R_m is the mass ablation rate; Δm is the mass difference of the samples prior to and after ablation; R_1 is the linear ablation rate; Δd is the thickness difference of the samples prior to and after ablation and t is the time of ablation. The coatings' oxidation investigations were done in the DSC METTLER TOLEDO TGA/DSC 1. The $10 \times 10 \times 10$ mm^3 specimens were transferred into the alumina crucible and heated in the air between 1500 °C and room temperature with heating rates of 5 °C min^{-1}.

The scanning electron microscopy (SEM) was applied to test the samples' chemical composition and morphology. The composition and phase analysis of the coating prior to and after ablation and oxidation were indicated using x-ray diffraction.

3. Results and Discussion

3.1 Microstructure Characterization

Figure 1(a) presents the surface of the SiC coating produced by the slurry sintering (SS). It could be found that no clear
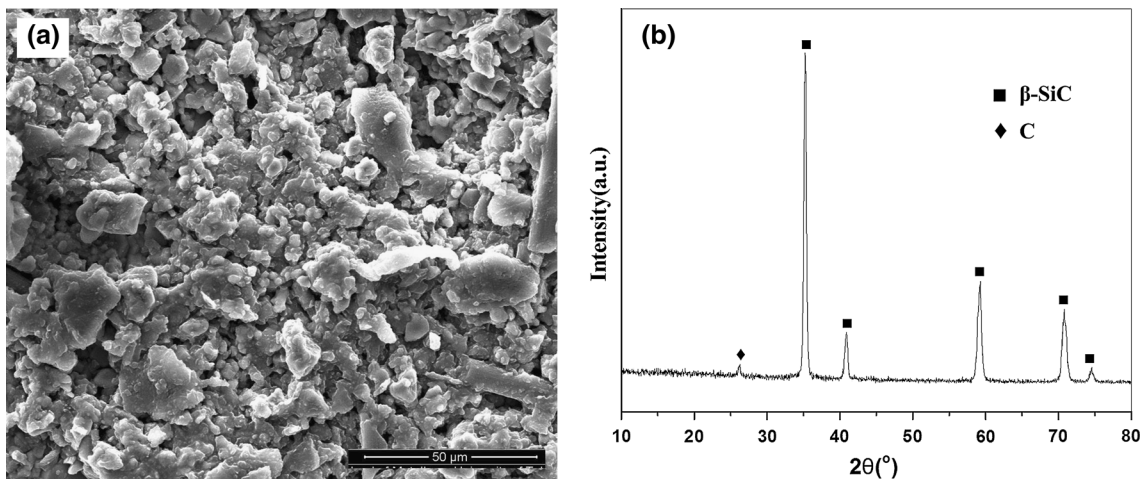

Fig. 1 X-ray patterns and SEM micrograph on the coating surface estimated in the slurry sintering methods
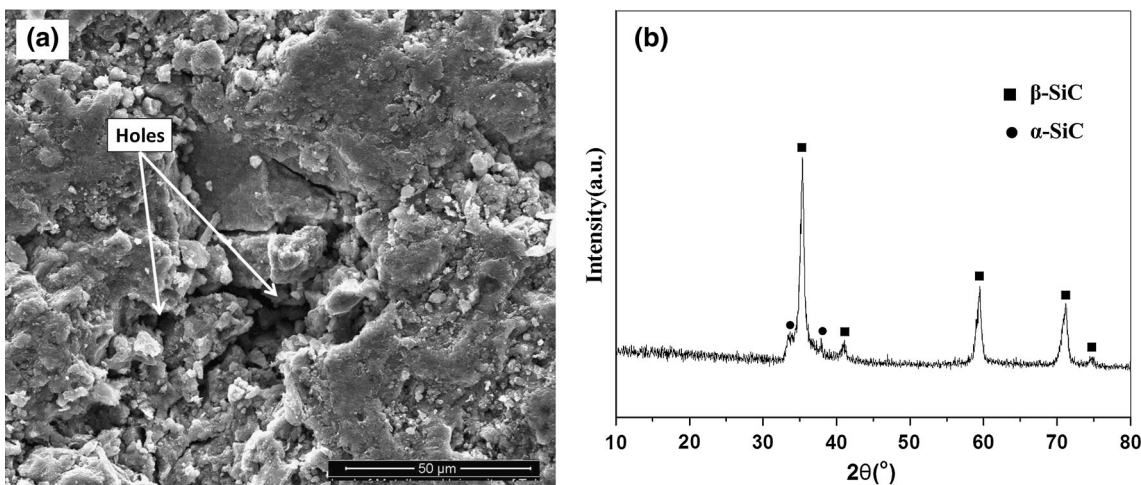

Fig. 2 X-ray patterns and SEM micrograph on the coating surface estimated in the pack cementation methods

cracks existed in the coating. In Fig. 1(b), robust peaks of β-SiC were observed, showing the reaction of carbon with silicon at the higher temperature and formed SiC on the graphite surface (Ref 17). The weak peak of carbon also appeared, indicating that SiC coating was not completely formed on the surface.

Figure 2 depicts the x-ray pattern and the microstructure of the SiC coating obtained through PC. There are some holes in the SiC coating (Fig. 2a). Oxygen can penetrate along these
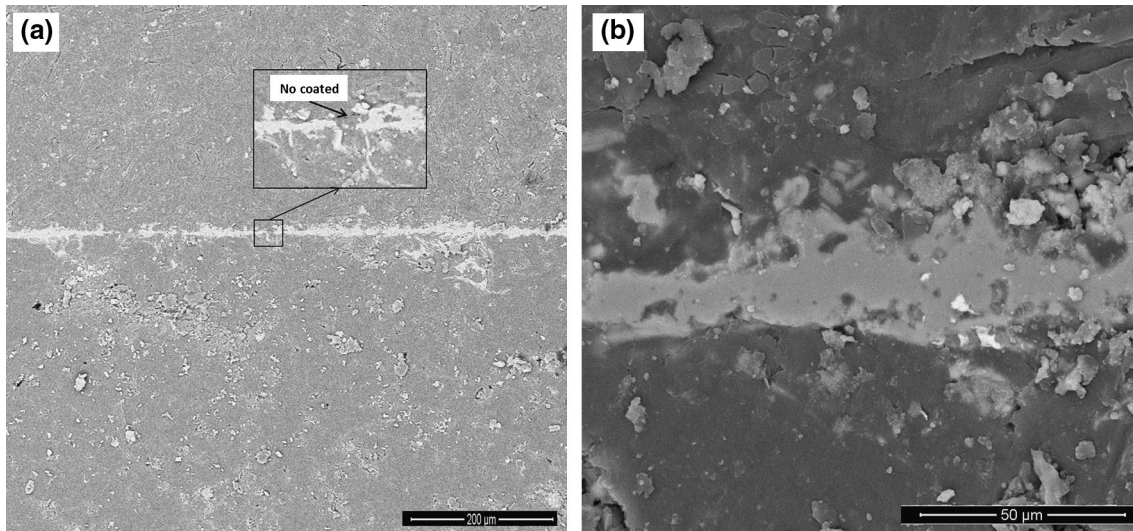
Fig. 3 SEM micrograph of the SS–SiC coating cross section in two magnifications
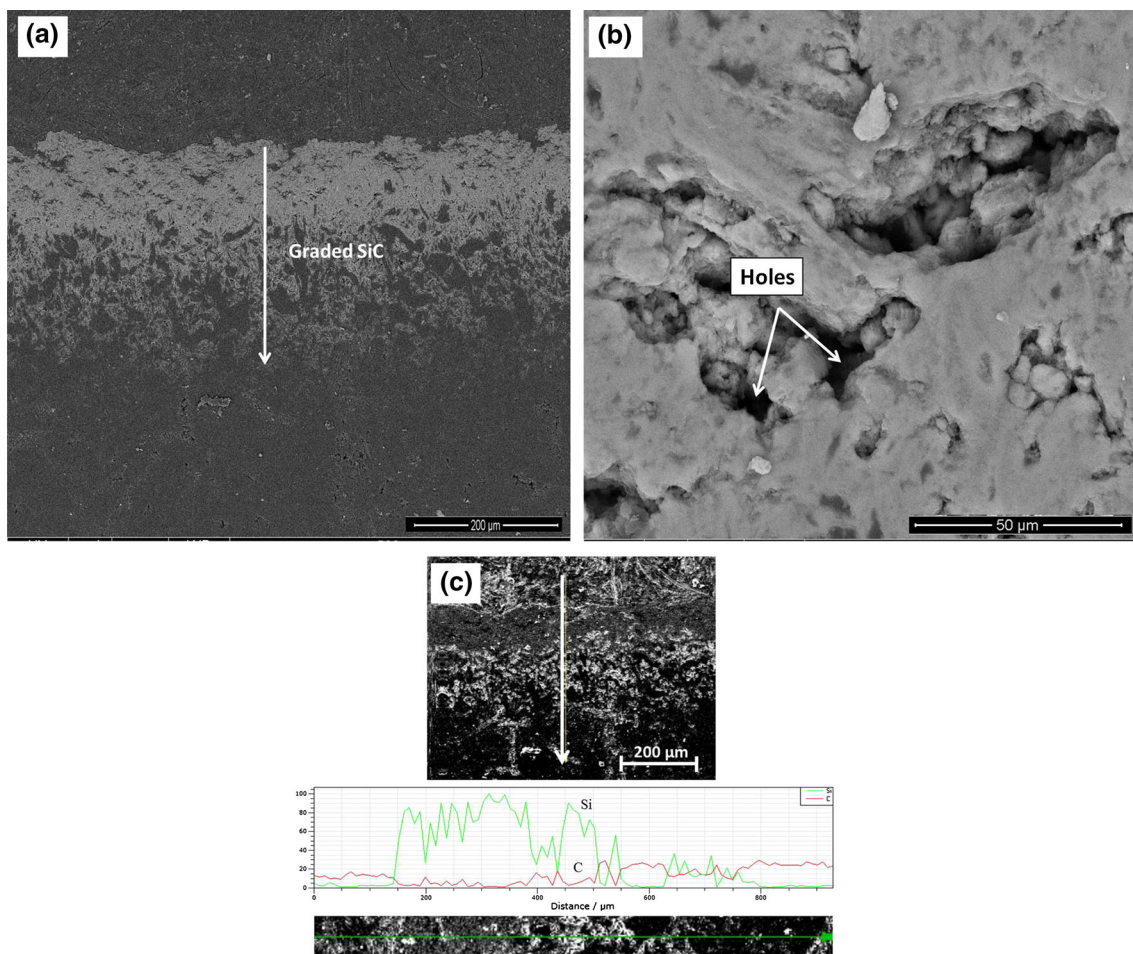
Fig. 4 SEM micrograph and element line scan analysis of the PC–SiC coating cross section: (a) low magnifications; (b) high magnifications; (c) EDS element line scan analysis
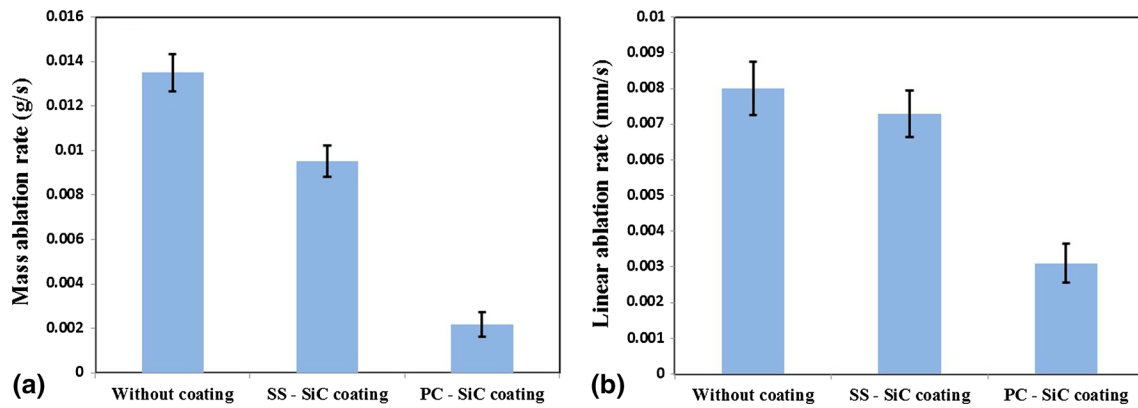
Fig. 5 The ablation rates of samples with and without SiC coating after ablation for 60 s: (a) mass ablation rates; (b) linear ablation rates
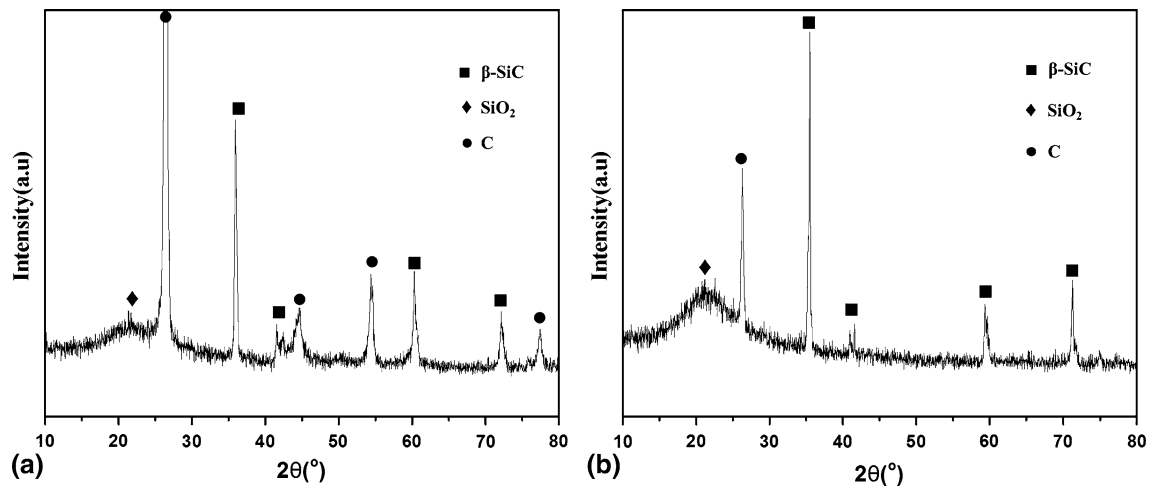

Fig. 6 The XRD pattern of the SiC coatings: (a) SS–SiC coating; (b) PC–SiC coating

holes and oxide the graphite substrate. Figure 2(b) displays only β-SiC and α-SiC peaks which show the successful formation of the coating on the substrate.

Cross-sectional images of the SS–SiC coating are shown in Fig. 3. The SS–SiC coating is thin with about 50 μm thicknesses (Fig. 3b) and in some places; the coating has not been formed as observed in Fig. 3(a).

At high temperature, silicon melts and penetrates into the voids in the graphite surface. In the next step, silicon reacts with carbon and forms SiC. The coating thickness depends on the silicon penetration rate and the reaction rate of silicon and carbon (Ref 25). At high temperatures, the reaction rate is higher than the silicon penetration rate and the molten silicon has not sufficient time to penetrate into the interior of the graphite before the penetration path is completely blocked (Ref 4). Therefore, it is a disadvantage for the formation of the thicker SiC coating. According to the above explanation, it can be concluded that sintering at 1700 °C is not suitable to obtain thick SiC gradient coating as shown in Fig. 3(a).

The pack cementation process is a usual method to produce SiC-graded coatings on the graphite (Ref 30). Cross-sectional images and element line scan analysis of the PC–SiC coating are shown in Fig. 4. Figure 4(a) displays the coating with around 500 μm thickness fabricated by the pack cementation method. There are also some voids in the PC–SiC coating
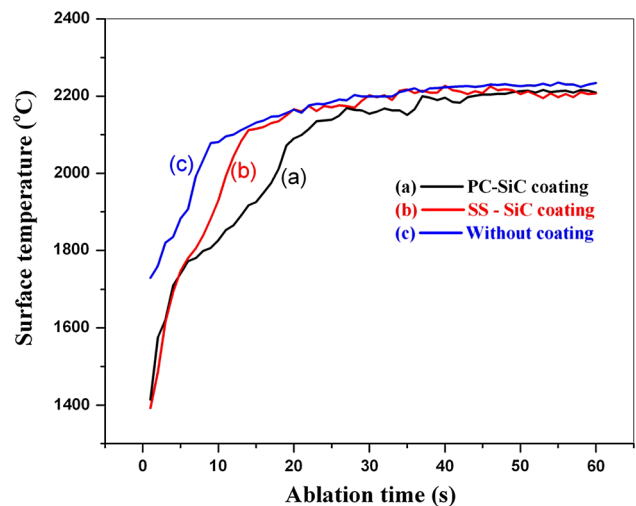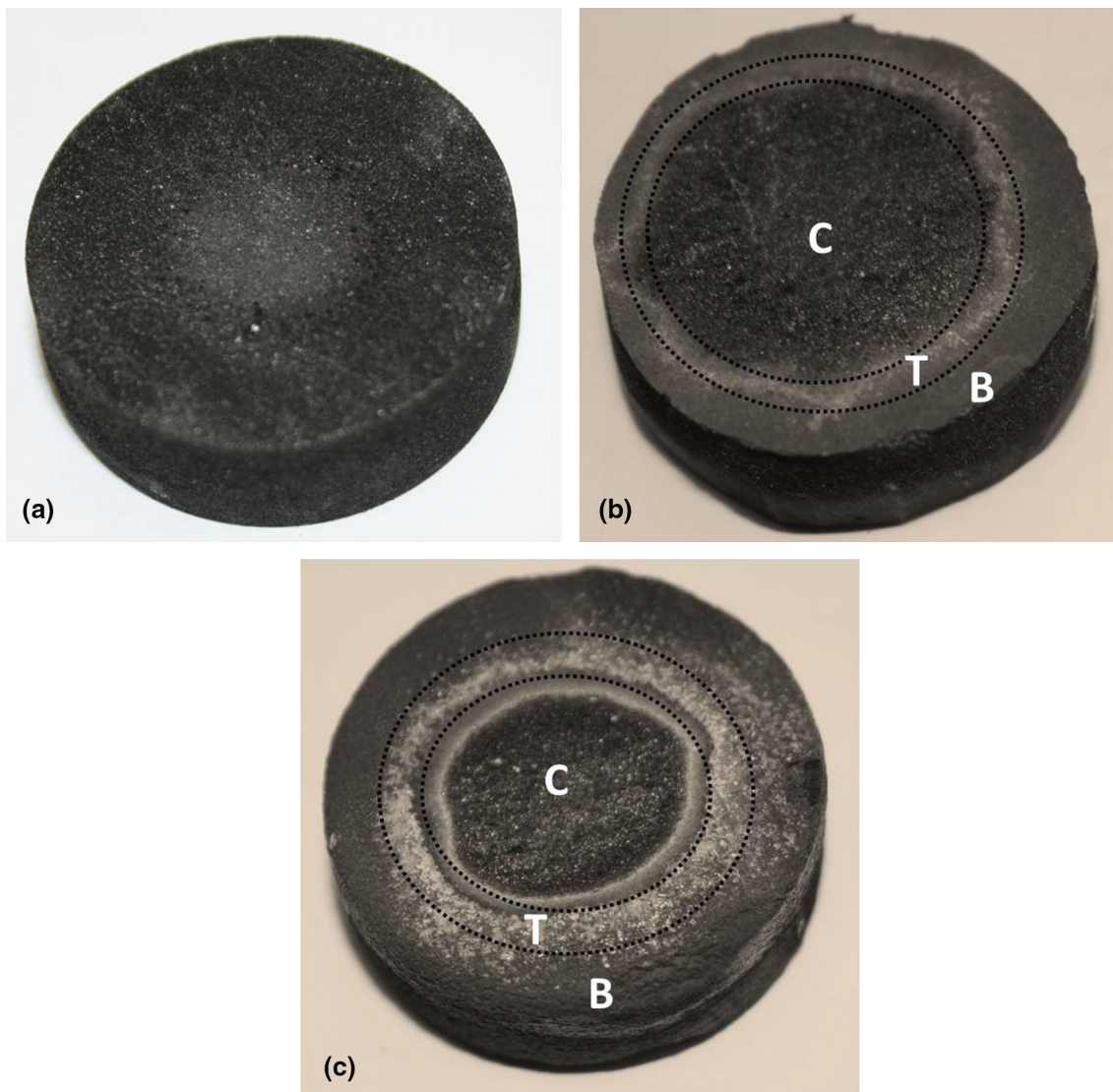

Fig. 7 The surface temperature variation of the ablation center

(Fig. 4b). According to the element line scanning result (Fig. 4c), the concentration of silicon decreased gradually from the surface to the inner of graphite substrate. It means that a SiC-graded coating was achieved in the pack cementation

Fig. 8 Macroscopic morphology of samples after ablation for 60 s: (a) without coating; (b) SS–SiC coating; (c) PC–SiC coating

process, which would produce a good thermal shock resistance for the coating (Ref 31).

### 3.2 Ablation Performance of Coatings

3.2.1 Ablation Properties. The mass and linear ablation rates of samples after ablation for 60 s are shown in Fig. 5. It is obvious that sample without coating has high ablation under the oxyacetylene flame. The mass and linear ablation rates of SS–SiC coating are 9.52×10^{-3} g s^{-1} and 7.3×10^{-3} mm s^{-1}, while those for PC–SiC coating are as 2.17×10^{-3} g s^{-1} and 3.1×10^{-5} mm s^{-1}. The PC–SiC coating considerably increased the ablation resistance in comparison to the SS–SiC coating.

Figure 6 reveals the surface XRD pattern of the SS–SiC and PC–SiC coating after ablation for 60 s. The coating after ablation was contained β-SiC, SiO$_2$ and carbon. Carbon peaks demonstrated that the graphite substrate was exposed to ablation in both coatings. The SiO$_2$ peaks were also found, which were produced by the oxidation of SiC. The β-SiC phase is probably due to the non-oxidized edges of the sample.

Figure 7 plots the surface temperature curve changed with increased ablation time. All samples' surface temperature elevated to the peak and remained at an almost fixed level. This is due to a heat balance between heating from the oxyacetylene flame and cooling processes from heat emission and transmission to the environment (Ref 32).

The uncoated graphite's temperature was more than the coated specimens. The heat release from the graphite oxidation is much higher than that from the SiC oxidation (Ref 28).

For the SS–SiC coating, the surface temperature quickly increases in the first 14 s. After 14 s, the temperature rises slowly and ultimately remains constant. For the PC–SiC coating, the surface temperature rises in the first 43 s but with a slower heating rate than that of the SS–SiC coating. Then, the temperature is kept constant. The temperature of the SS–SiC coating surface was more than the PC–SiC coating until 43 s. Hence, the thin SS–SiC coating vanished easily at the ablation's initial stage. In the following, the graphite substrate is oxidized. However, the thick PC–SiC coating can resist ablation for a long time. After 43 s, the temperature is almost an equal value for both samples.
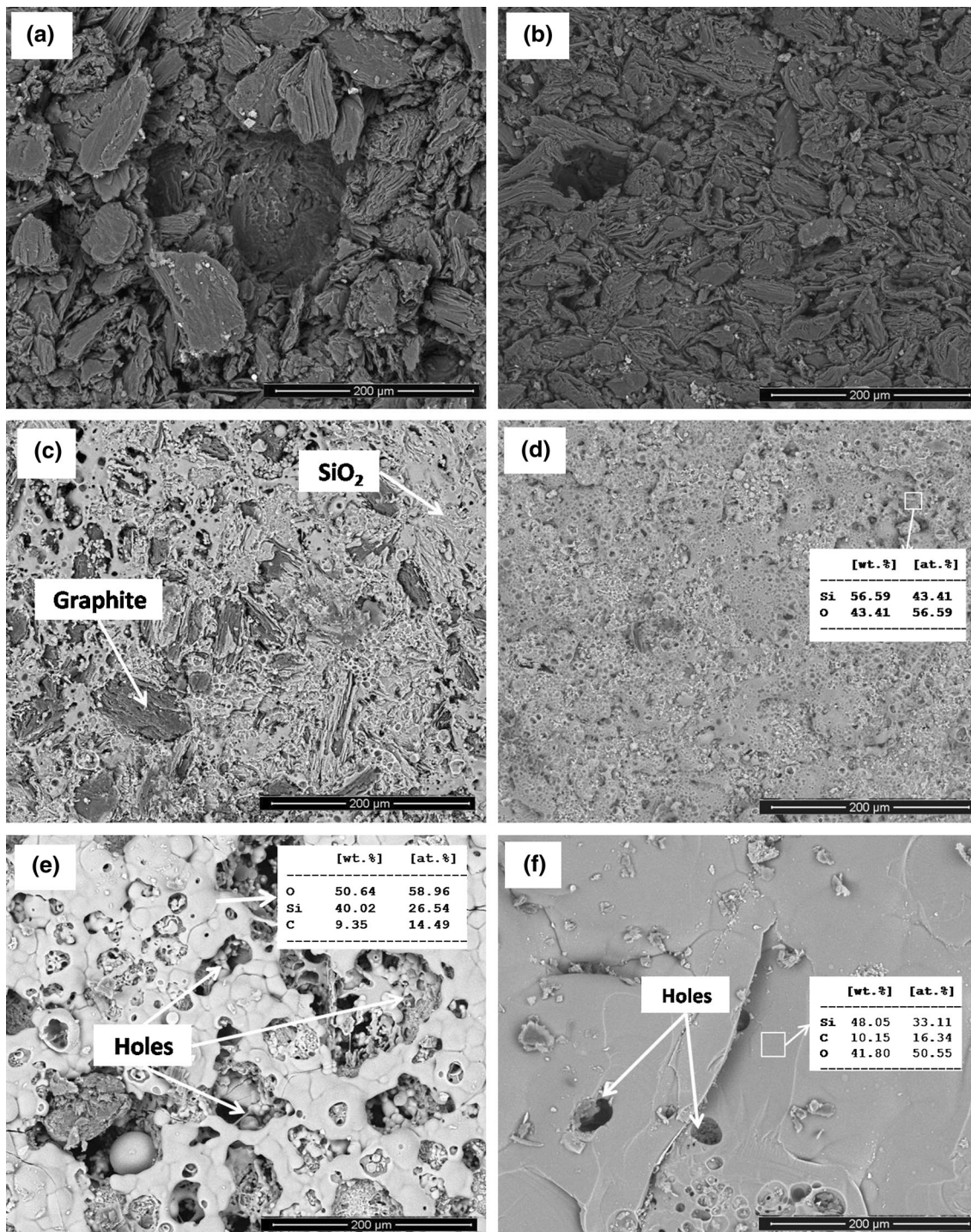
Fig. 9 Surface morphologies of coatings after ablation for 60 s under the oxyacetylene flame: (a) central ablation region of SS–SiC coating; (b) central ablation region of PC–SiC coating; (c) transitional ablation region of SS–SiC coating; (d) transitional ablation region of PC–SiC; (e) border ablation region of SS–SiC coating; (f) border ablation region of PC–SiC coating

3.2.2 Ablation Morphology. Figure 8 depicts the surface's macroscopic morphology in the ablation test after 60 s. Three areas exist after ablation on the coating surface: border region (B), transition region (T) and central region (C). There is an obvious hole in the center, showing that the graphite matrix was subjected because of the ablation. Compared with Fig. 8(c), the hole diameter is larger in Fig. 8(b), showing that

the PC–SiC coating can save the graphite under the oxyacetylene flame from ablation for 60 s compared with SS–SiC coating. Figure 9 shows the morphologies of the SiC coatings after ablation for 60 s. Figure 9(a) and (b) displays the central ablation region's microscopic morphology for SS–SiC and PC–SiC coatings after ablation. The graphite matrix was exposed in both samples. Figure 9(c) and (d) depicts in the transition
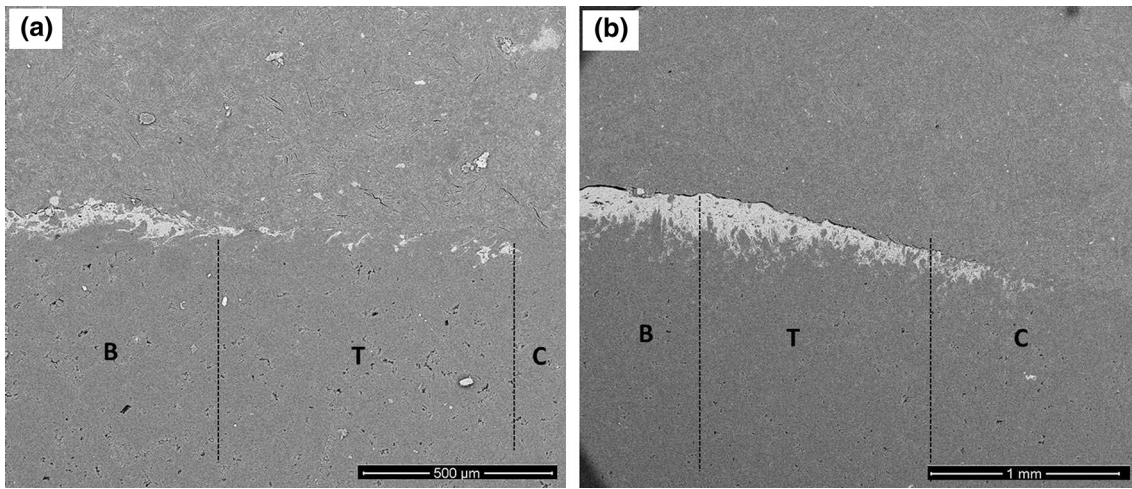
Fig. 10 Cross section of the coatings after ablation for 60 s under the oxyacetylene flame: (a) SS–SiC coating; (b) PC–SiC coating
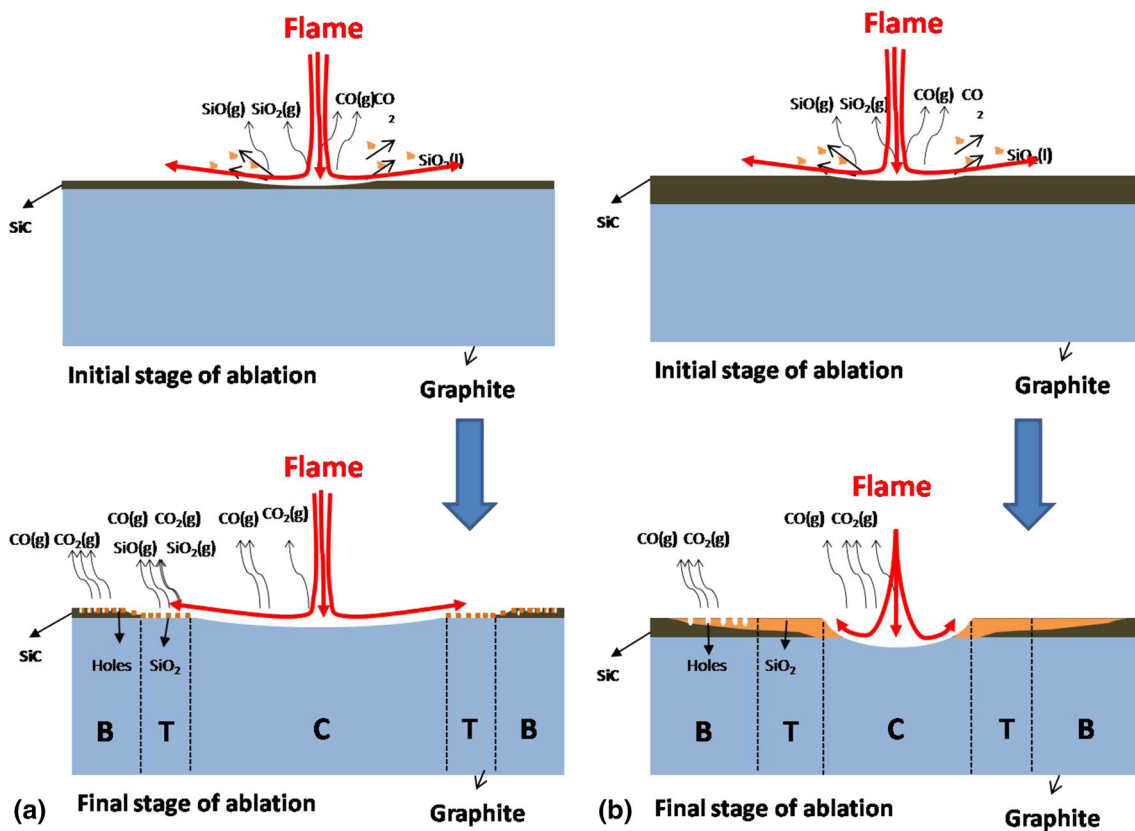

Fig. 11 The schematic of the SiC coating during the ablation: (a) SS–SiC coating (b) PC–SiC coating

region the microstructure. The region of transition of the coating possesses lower temperature and pressure by a distance from the flame center, compared to the center. Hence, the impact of ablation behaviors declines (Ref 33). Figure 9(c) shows that a part of SiO_2 is denudated from the surface by air flow after SiC coating of the sample surface is oxidized. It is believed that SS–SiC coating cannot form a dense oxide layer

and its ablation resistance is weak. For the PC–SiC coating (Fig. 9d), SiO_2 generates a thick protective layer to prevent ablation in the transition region.

Figure 9(e) and (f) shows the morphology of the border region. As shown in Fig. 9(e), the surface of the SS–SiC coating is covered with a white glassy layer. According to EDS analysis and XRD pattern (Fig. 6), the white layer can be
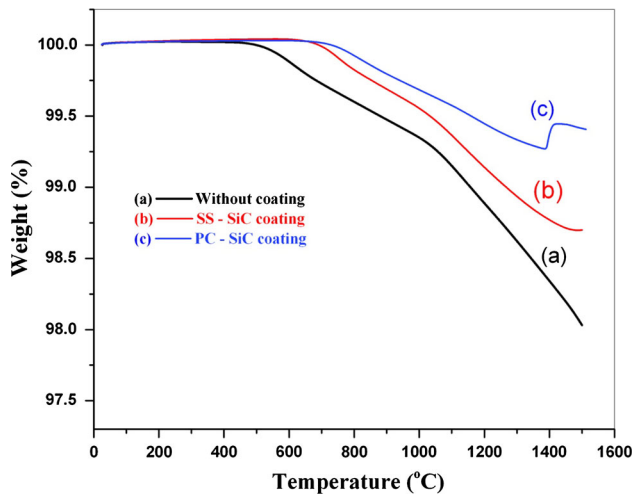
Fig. 12 TGA curve of (a) without coating: (b) SS–SiC coating and (c) PC–SiC coating

related to SiO_2. Some holes exist in the coating, which may be attributed to the escape of gases (Ref 7). The layer of oxide SiO_2 made on the PC–SiC coating surface (Fig. 9f), with fewer holes, is denser than the SS–SiC coating, leading to higher oxidation resistance compared to the SS–SiC coating.

Figure 10 displays cross section of the coating after ablation. Three ablation regions are indicated in the image. It is evident that the SiO_2 layer generated from the PC–SiC coating is continues, while it for SS–SiC coating is discontinues. The continuous SiO_2 layer creates a sealing mechanism which can protect the graphite effectively.

3.2.3 Ablation Mechanism. Ablation is a combination of mechanical denudation and chemical reaction (Ref 34). In the tests of oxyacetylene torch ablation, the reactions below might occur (Ref 28, 29)

$$SiC(s) + 2O_2 \rightarrow SiO_2(s) + CO_2(g) \tag{Eq 3}$$

$$2SiC(s) + 3O_2(g) \rightarrow 2SiO_2(s) + 2CO(g) \tag{Eq 4}$$
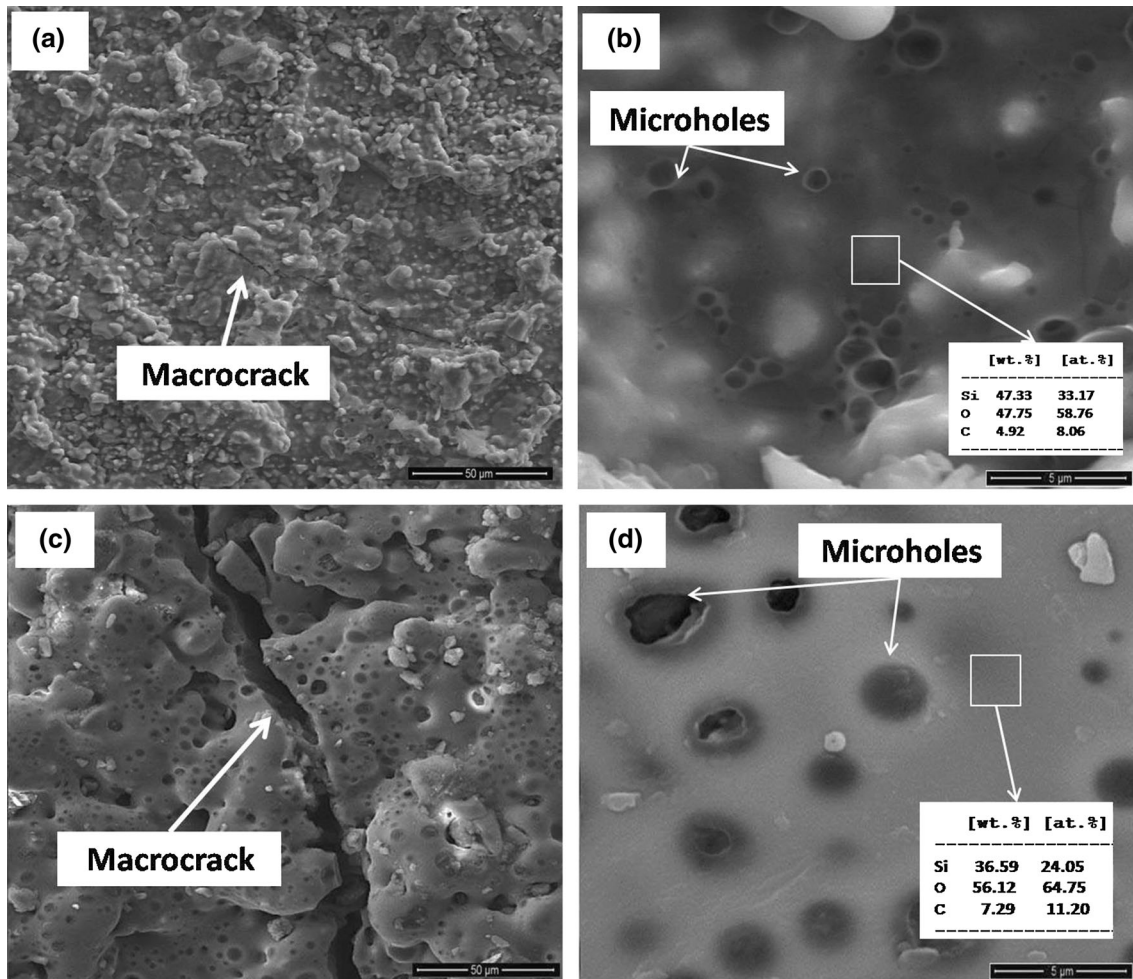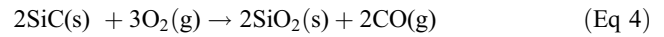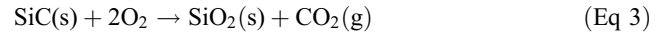
Fig. 13 SEM image of the coatings after the TGA test: (a, b) SS–SiC coating; (c, d) PC–SiC coating
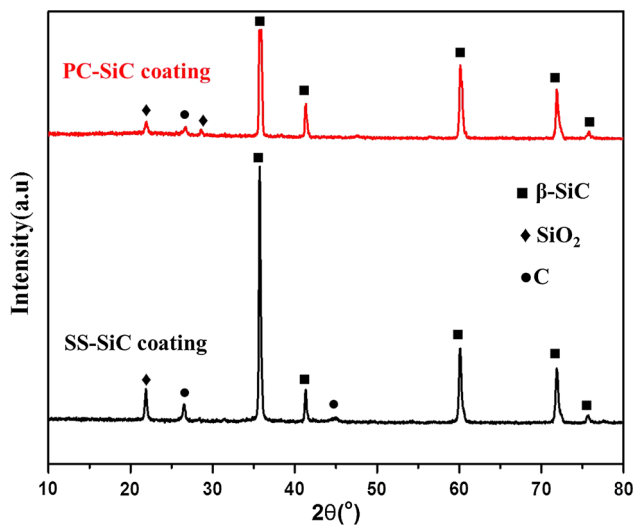
Fig. 14 The XRD pattern of the SS–SiC and PC–SiC coating after the TGA test

$$SiO_2(s) \rightarrow SiO_2(l) \qquad\qquad (Eq\ 5)$$

$$SiO_2(l) \rightarrow SiO_2(g) \qquad\qquad (Eq\ 6)$$

$$SiO_2(l) + CO(g) \rightarrow SiO(g) + CO_2(g) \qquad (Eq\ 7)$$

$$C(s) + O_2(g) \rightarrow CO_2(g) \qquad\qquad (Eq\ 8)$$

$$2C(s) + O_2(g) \rightarrow 2CO(g). \qquad\qquad (Eq\ 9)$$

Figure 11 shows the ablation schematic of the SiC coating. The SiC coating reacts with oxygen in the first phase of ablation, and SiO_2 i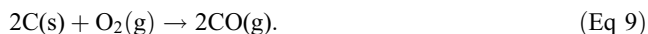s generated rapidly on the surface of coating based on reactions 3 and 4. In the center of the sample, SiO_2 melt (Eq 5) blew away by high-speed gas flow. With further oxidation, liquid SiO_2 vaporizes (Eq 6 and 7) as a result of high temperature (> 2000 K) (Ref 35).

Nevertheless, the pressure and temperature declined noticeably by a distance from the surface's center. As a result, in the final stage of ablation, three distinct regions (central region (C), transitional region (T) and border region (B)) formed on the surface. In the central region, all of the SiC is consumed according to reaction 3–7 under the ultra-high temperature and high-speed gas flow. The graphite substrate is oxidized based on reactions 8 and 9. The mechanical denudation and chemical ablation are the major mechanisms on the central area.

The temperature of ablation is less in the transition area; however, it is more compared to the SiO_2 melting point. SiO_2 exists as molten film. The continuous molten film of SiO_2 generated from the PC–SiC oxidation renders a mechanism of sealing that is able to operate as an obstacle against the oxygen diffusion and resistant against more coating ablation. Nevertheless, the discontinuous SiO_2 film made from the thin SS–SiC may not constructively preserve the graphite, and the chemical ablation is the major mechanism on the transition area.

The temperature of ablation is lower on the border and SiO_2 as a solid phase based on reactions 3 and 4. Some of the holes were made, due to CO or CO_2 release. CO_2 and CO produced at high temperature via SiC and the graphite substrate oxidation (Eq 3, 4, 8, and 9). The border area is far from the central area, and the air flow of ablation is the weakest. Thus, on the border,

mechanical denudation does not exist. The solid-state chemical ablation is the main mechanism on the border region.

3.3 Oxidation Performance of Coatings

Figure 12 presents the TGA curves for coated and uncoated graphite heated between room temperature and 1500°. It is obvious that without the SiC coating, the sample weight is lost largely from 25 to 1500 °C and its weight loss percentage was up to 2.2% after TGA. This is while after coating, samples possessed excellent oxidation protection ability during the whole TGA and weight losses of SS–SiC and PC–SiC coatings are down to 1.3 and 0.6%, respectively. The uncoated sample began to become oxidized at about 500 °C and decrease weight. However, the oxidation temperature shifts to 660 and 720 °C for SS–SiC coating and PC–SiC coating, respectively. So, the coating of SiC on the substrate, in particular, for the coating of PC–SiC (Fig. 4), improved its oxidation resistance.

According to reactions 8 and 9, the oxidation reactions of graphite are a weight-decreasing process, while those of SiC coatings are a weight-increasing process (Eq 3 and 4) (Ref 21). From 660 to 1450 °C, the SS–SiC coating and from 720 to 1390 °C, the PC–SiC coating gradually lost weight, indicating oxidation of the graphite substrate that occurred due to the formation of macrocracks in the coating during the TGA test. Figure 13 presents the coatings' SEM images after oxidation. The cracks were found with large sizes on the surface (Fig. 13a and c), owing to the CTE mismatch among the graphite substrate and coating. When the coating was applied at high temperature, large thermal stress generated and resulted in the cracks (Ref 22).

The weight reduction of SS–SiC coating samples ended from 1450 to 1500 °C. SiC coating samples obtained weight at high temperature, owing to the coating materials' oxidation based on reactions 3 and 4. Nevertheless, the weight gain rate of coating materials and the substrate's weight loss rate were equal. So, the weight is kept almost with no change. The PC–SiC coating sample indicated increasing weight from 1390 to 1420 °C due to SiO_2 glass formation. More oxidation occurred by oxidative gases' diffusion along the oxide layer and reaction with SiC and carbon at the interface of oxide/SiC (Ref 36), and thus weight loss after 1420 °C.

Figure 13(b) and (d) shows high-magnification surface images of SiC coating after oxidation. The samples were covered by a glass layer, which is identified as SiO_2 according to XRD (Fig. 14) and EDS results (Fig. 13b and d). Some holes were formed on the surface, owing to the release of CO or CO_2. The presence of these holes acts as a path for oxidative gases to reach the carbon surface (Ref 36).

4. Conclusion

1. SiC coatings were produced on graphite by pack cementation (PC) and slurry sintering (SS). The PC coating was the functionally graded coating with about 500 μm thickness and the thickness of SS coating was 50 μm.
2. The mass ablation rates of the SS–SiC and PC–SiC coatings decreased compared with the uncoated samples, which was mainly attributed to the formation of a SiO_2 layer on the surface.

3. The PC–SiC coating elevated considerably the ablation resistance in comparison to the SS–SiC coating. The continuous SiO_2 molten film formed via the PC–SiC oxidation generates a sealing mechanism which can be an obstacle against the oxygen diffusion and hinder more ablation. This is while discontinuous SiO_2 film formed from the thin SS–SiC cannot protect the graphite effectively.

4. The non-isothermal oxidation test showed that the SiC coating played an effective role in increasing the oxidation resistance of the graphite from room temperature to 1500 °C.

5. The TGA showed that the uncoated sample began to become oxidized at about 500 °C and decrease weight. However, the oxidation temperature shifts to 660 and 720 °C for SS–SiC coating and PC–SiC coating, respectively.

6. The oxidation of the graphite substrate occurred due to the formation of macrocracks in the coating during the TGA and also the formation of holes on SiO_2 glass layer owing to release of CO or CO_2.

References

1. D.D.L. Chung, Review Graphite, *J. Mater. Sci.*, 2002, **37**, p 1475–1489

2. A. Abdollahi, N. Ehsani, Z. Valefi, and A. Khalifesoltani, SiC Nanoparticles Toughened-SiC/MoSi₂-SiC Multilayer Functionally Graded Oxidation Protective Coating for Carbon Materials at High Temperatures, *J. Mater. Eng. Perform.*, 2017, **26**, p 2878–2889

3. P. Wang, W. Han, X. Zhang, N. Li, G. Zhao, and S. Zhou (ZrB₂–SiC)/SiC Oxidation Protective Coatings for Graphite Materials, *Ceram. Int.*, 2015, **41**(5), p 6941–6949

4. Q.S. Zhu, X.L. Qiu, and C.W. MA, Oxidation Resistant SiC Coating for Graphite Materials, *Carbon*, 1999, **37**, p 1475–1484

5. Q.G. Fu, H.J. Li, K.Z. Li, and X.H. Shi, Microstructure and Oxidation Protective Ability of MoSi₂-SiC-Si Coating Toughened with SiC Whiskers for Carbon/Carbon Composites, *Surf. Eng.*, 2008, **24**, p 383–387

6. B. Paul, J. Prakash, and P.S. Sarkar, Formation and Characterization of Uniform SiC Coating on 3-D Graphite Substrate Using Halide Activated Pack Cementation Method, *Surf. Coat. Technol.*, 2015, **282**, p 61–67

7. C. Sun, H.J. Li, Q.G. Fu, J.P. Zhang, and H. Peng, Double SiC Coating on Carbon/Carbon Composites Against Oxidation by a Two-Step Method, *Trans. Nonferrous Metal. Soc.*, 2013, **23**(7), p 2107–2112

8. S. Aliakbarpour, M. Zakeri, M.R. Rahimipour, and R. Irankhah, Effect of SiC-Mullite Coatings on Oxidation Resistance of Graphite, *Adv. Appl. Ceram.*, 2014, **113**, p 358–361

9. J.F. Huang, B. Wang, H.J. Li, M. Liu, L.Y. Cao, and C.Y. Yao, A MoSi₂/SiC Oxidation Protective Coating for Carbon/Carbon Composites, *Corros. Sci.*, 2011, **53**, p 834–839

10. H.J. Li, T. Feng, Q.G. Fu, H. Wu, and X.T. Shen, Oxidation and Erosion Resistance of MoSi₂–CrSi₂–Si/SiC Coated C/C Composites in Static and Aerodynamic Oxidation Environment, *Carbon*, 2010, **48**, p 1636–1642

11. Q.G. Fu, H.J. Li, Y.J. Wang, K.Z. Li, and X.H. Shi, B₂O₃ Modified SiC–MoSi₂ Oxidation Resistant Coating for Carbon/Carbon Composites by a Two-Step Pack Cementation, *Corros. Sci.*, 2009, **51**, p 2450–2454

12. X. Yang, Q.Z. Huang, Z.A. Su, X. Chang, L.Y. Chai, C.X. Liu, L. Xue, and D. Huang, Resistance to Oxidation and Ablation of SiC Coating on Graphite Prepared by Chemical Vapor Reaction, *Corros. Sci.*, 2013, **75**, p 16–27

13. X. Yang, Q.Z. Huang, Z.A. Su, L.Y. Chai, X.F. Wang, and L.P. Zhou, A Double Layer Nanostructure SiC Coating for Anti-oxidation Protection of Carbon/Carbon Composites Prepared by Chemical Vapor Reaction

14. and Chemical Vapor Deposition, *Ceram. Int.*, 2013, **39**, p 50535–55062

14. Q.G. Fu, H.J. Li, X.H. Shi, K.Z. Li, and G.D. Sun, Silicon Carbide Coating to Protect Carbon/Carbon Composites Against Oxidation, *Scr. Mater.*, 2005, **52**, p 923–927

15. J.F. Huang, X.R. Zeng, H.J. Li, X.B. Xiong, and Y.W. Fu, Influence of the Preparation Temperature on the Phase Microstructure and Anti-Oxidation Property of a SiC Coating for C/C Composites, *Carbon*, 2004, **42**, p 1517–1521

16. C.C.M. Ma, N.H. Tai, and W.C. Chang, Microstructure and Oxidation Resistance of SiC Coated Carbon-Carbon Composites via Pressureless Reaction Sintering, *J. Mater. Sci.*, 1995, **31**, p 649–654

17. J. Zhao, G. Wang, Q.G. Guo, and L. Liu, Microstructure and Property of SiC Coating for Carbon Materials, *Fusion Eng. Des.*, 2007, **82**, p 363–368

18. M.H. Hu, K.Z. Li, H.J. Li, B. Wang, and H.L. Ma, Double layer ZrSi₂-ZrC-SiC/SiC Oxidation Protective Coating for Carbon/Carbon Composites, *Surf. Eng.*, 2015, **31**, p 335–341

19. L. Li, H.J. Li, H.J. Lin, L. Zhuang, S.L. Wang, T. Feng, X.Y. Yao, and Q.G. Fu, Comparison of the Oxidation Behaviors of SiC Coatings on C/C Composites Prepared by Pack Cementation and Chemical Vapor Deposition, *Surf. Coat. Technol.*, 2016, **302**, p 56–64

20. J.Y. Jing, Q.G. Fu, and R.M. Yuan, Nanowire-Toughened CVD-SiC Coating for C/C Composites with Surface Pre-oxidation, *Surf. Eng.*, 2018, **34**, p 47–53

21. M.H. Hu, K.Z. Li, H.J. Li, T. Feng, and L. Li, Influence of β-SiC on the Microstructures and Thermal Properties of SiC Coatings for C/C Composites, *Surf. Coat. Technol.*, 2016, **304**, p 188–194

22. H.J. Li, Y.J. Wang, Q.G. Fu, and G.D. Sun, Improvement in Oxidation Properties of SiC-Coated Carbon/Carbon Composites Through Modification of the SiC/Carbon Interface, *Surf. Coat. Technol.*, 2014, **245**, p 49–54

23. X.F. Qiang, H.J. Li, Y.L. Zhang, D.J. Yang, L.J. Guo, and J.F. Wei, Fabrication and Thermal Shock Resistance of in situ SiC Nanowire-SiC/SiC Coating for Carbon/Carbon Composites, *Corros. Sci.*, 2012, **59**, p 343–347

24. Y.H. Chu, Q.G. Fu, H.J. Li, K.Z. Li, X. Zou, and C.G. Gu, Influence of SiC Nanowires on the Properties of SiC Coating for C/C Composites Between Room Temperature and 1500 °C, *Corros. Sci.*, 2001, **53**, p 3048–3053

25. Z.J. Liu, Q.G. Guo, L. Liu, J.L. Shi, and G.T. Zhai, Effect of Sintering Temperature on Microstructure and Properties of SiC Coatings for Carbon Materials, *Surf. Coat. Technol.*, 2008, **202**, p 3094–3099

26. Juan Zhao, Lang Liu, Quangui Guo, Jingli Shi, and Gengtai Zhai, Oxidation Protective Behavior of SiC/Si–MoSi₂ Coating for Different Graphite Matrix, *Mater. Lett.*, 2006, **60**, p 1964–1967

27. T. Wu, W. Wei, and S. Hsu, The Effect of Boron Additive on the Oxidation Resistance of SiC-Protected Graphite, *Ceram. Int.*, 1992, **18**, p 167–172

28. B.Q. Li, P.C. Kang, H.S. Gou, G.H. Wu, and S. Mula, Surface Morphology Evolution and Ablation Mechanism of SiC–Si Multiphase Ceramic Coating on Graphite Under Oxyacetylene Flame, *Corros. Sci.*, 2014, **88**, p 473–480

29. C. Ni, K. Li, L. Liu, H. Li, Q. Fu, L. Guo, and N. Liu, Ablation Mechanism of SiC Coated C/C Composites at 0° Angle in Two Flame Conditions Under an Oxyacetylene Flame, *Corros. Sci.*, 2014, **84**, p 1–10

30. H. Jafari, N. Ehsani, S.A. Khalifeh-Soltani, and M. Jalaly, Nano-SiC/SiC Anti-oxidant Coating on the Surface of Graphite, *Appl. Surf. Sci.*, 2013, **264**, p 128–132

31. H.J. Li, G.S. Jiao, K.Z. Li, and C. Wang, Multilayer Oxidation Resistant Coating for SiC Coated Carbon/Carbon Composites at High Temperature, *Mater. Sci. Eng. A*, 2008, **475**, p 179–184

32. Y.J. Wang, H.J. Li, Q.G. Fu, H. Wu, L. Liu, and C. Sun, Ablation Behavior of TaC Coating on SiC Coated C/C Composites at Different Temperature, *Ceram. Int.*, 2013, **39**, p 359–365

33. Z.Q. Li, H.J. Li, W. Li, J. Wang, S.Y. Zhang, and J. Guo, Preparation and Ablation Properties of ZrC–SiC Coating for Carbon/Carbon Composites by Solid Phase Infiltration, *Appl. Surf. Sci.*, 2011, **258**, p 565–571

34. D. Zhao, C.R. Zhang, H.F. Hu, and Y.D. Zhang, Ablation Behavior and Mechanism of 3D/ZrC Composite in Oxyacetylene Torch Environment, *Compos. Sci. Technol.*, 2011, **71**, p 1392–1396

35. Y. Xiang, W. Li, S. Wang, and Z.H. Chen, The Effect of Zirconium Carbide on Ablation of SiC-Coated Carbon/Silicon Carbide Composites Under an Oxy-acetylene Flam, *Int. J. Appl. Ceram. Technol.*, 2014, **11**, p 558–567

36. S. Farhan, R.M. Wang, and K.Z. Li, Characterization of Latticed SiC Nanowires Containing Coating for Carbon Foam Using Carbonization Activated Pack Cementation Process, *J. Alloy. Compd.*, 2016, **682**, p 695–705